Journal of Colloid and Interface Science 539 (2019) 161–167

Contents lists available at ScienceDirect

Journal of Colloid and Interface Science

journal homepage: www.elsevier.com/locate/jcis

Regular Article

One-pot green synthesis of bimetallic hollow palladium-platinum nanotubes for enhanced catalytic reduction of p-nitrophenol

Yinan Wang [a,b], Qingchuan Li [b], Ping Zhang [a], David O'Connor [a], Rajender S. Varma [c], Miao Yu [b,*], Deyi Hou [a,*]

[a] School of Environment, Tsinghua University, Beijing 100084, China
[b] School of Chemical Engineering and Technology, Harbin Institute of Technology, 92 West Da-Zhi Street, Harbin 150001, China
[c] Regional Centre of Advanced Technologies and Materials, Faculty of Science, Palacky University, Šlechtitelů 27, 783 71 Olomouc, Czech Republic

GRAPHICAL ABSTRACT

Bimetallic hollow PdPt nanotubes was fabricating in a facile and green route for enhancing catalytic reduction of *p*-nitrophenol.

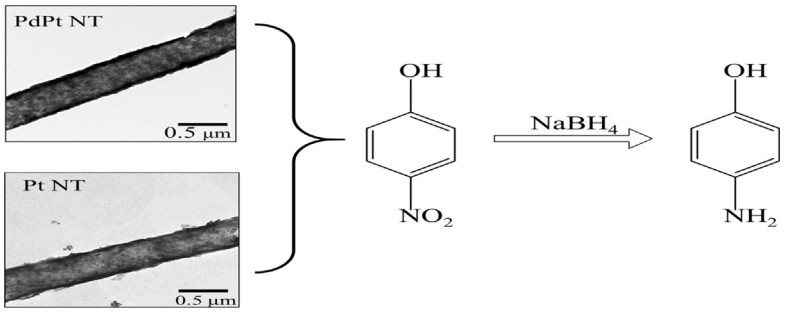

ARTICLE INFO

Article history:
Received 13 November 2018
Revised 13 December 2018
Accepted 14 December 2018
Available online 15 December 2018

Keywords:
Green synthesis
Lipid tubules
PdPt nanotube
Synergistic effect
p-nitrophenol reduction

ABSTRACT

Bimetallic alloy nanostructures have garnered much attention due to their unique performances in catalytic processes. However, decline in catalytic activity over the life span has been a protracted limitation, ascribed largely to the aggregation or dissociation of particles and still remains a challenge for manufacturing bimetallic nanostructures of sufficient stability. Herein, a surfactant- and solvent-free greener strategy is presented for the fabrication of bimetallic palladium-platinum (PdPt) nanotubes (NTs), deploying lipid tubules as template and ascorbic acid as a reducing agent; the ensuing NTs comprise crystalline tubal nanostructures of ~12 μm length, ~500 nm cross-sectional diameter, and ~57 nm tube wall thickness. When used for the catalytic reduction of *p*-nitrophenol (PNP), the PdPt NTs delivered improved kinetic apparent rate constants (k_{app}) compared to Pt NTs (0.5 min^{-1} *vs.* 0.2 min^{-1}). Moreover, the NTs demonstrated high stability when used over multiple catalytic cycles thus opening up new potential routes for the fabrication of alloy NTs using lipid tubules as templates.

1. Introduction

Remediation efforts are required [1–3] in order to protect the environment and human health from organic [4] and heavy metal [5,6] pollutants. The fabrication of bimetallic nanostructures has drawn considerable attention due to unique physicochemical

E-mail addresses: miaoyu_che@hit.edu.cn (M. Yu), houdeyi@tsinghua.edu.cn (D. Hou).

https://doi.org/10.1016/j.jcis.2018.12.053
0021-9797/

properties in distinctive catalytic applications [7]. Synergistic effects emanating from bimetallics holds advantages over monometallic catalysts [8,9] in nitric oxide (NO) reduction [8], carbon monoxide (CO) oxidation [10], glycerol oxidation [11], and the chemical reduction of nitrophenols [12] such as *p*-nitrophenol.

PNP has been used for the production of pesticides, insecticides, herbicides, pharmaceuticals, and explosives [13]. However, as a potential carcinogen, the US Environmental Protection Agency regards PNP to be a hazardous material and its use is now restricted in the US [14]. Consequently, the detection of PNP in the environment has caused widespread concern in recent years [14]. PNP pollution has been found to have its origin from its manufacture stage. As such, several techniques have been developed for PNP removal from industrial wastewater, including activated carbon sorption [15], microwave-assisted catalytic oxidation [16], microbial degradation [17], photocatalytic degradation [18], electro-Fenton methods [19], electrocoagulation [20], and electrochemical treatment [21]. However, since these techniques involve high energy consumption and/or the use of environmentally harmful chemical reagents, it is necessary to explore new PNP removal methods.

The prowess of bimetallic nanostructures in accelerating the reduction of PNP has been explored [22,23] as exemplified by the case of platinum (Pt) enhancing the catalytic activity of gold (Au) nanoparticles for PNP reduction [9]. Nevertheless, the aggregation of PtAu nanoparticles, and the requirement for catalyst support has limited their application [14] although stabilizing agents may help circumvent aggregation to some extent [24,25]. However, in order to maximize the catalytic activity of bimetallic nanostructures, the use of stabilizing agents is not desirable, as they can alter or block surface active sites [26]. Additionally, there is growing interest in the use of green and sustainable practices [27–29], in view of the fact that conventional synthesis methods for nanostructures often use hazardous reagents, including organic solvents, toxic chemicals and non-biodegradable surfactants [30,31], besides high energy input.

Lipid tubule templates offer a promising route to synthesize nanotubes (NTs) with controllable physical dimensions for catalysis applications [32–37]. The hydrophilic nature of their membrane surfaces provide an excellent environment for chemical reactions such as electroless plating to take place, thus leading to hollow tubule structures being inherited after template removal. Besides, the fabrication of lipid tubules is rapid and easy removal. Herein, we report a facile wet-chemical method for the synthesis of unsupported PdPt NTs using lipid tubule templates (Scheme 1). Unlike previous methods that require organic surfactants or the use of polymeric stabilizers at elevated temperatures, this synthesis protocol is conducted at ambient temperature and without the use of surfactants or solvents. The ensuing PdPt NTs display high catalytic activity for PNP reduction. This synthesis method holds great promise in view of the following: (1) the route is facile, greener and easy to adapt for large-scale production; (2) the assembled NT structures have high specific surface area and low aggregation potential; (3) the PdPt NTs are uniform in compositional distribution of Pd and Pt components, affording good catalytic performance. Furthermore, this approach opens up potential new routes for the development of other bimetallic or multi-metallic alloy NTs.

2. Experimental section

2.1. Materials

Palladium chloride ($PdCl_2$) and chloroplatinic acid ($H_2PtCl_6{\cdot}6H_2O$) were purchased from Shenyang Jinke reagents (China). Ascorbic acid and sodium borohydride ($NaBH_4$) were purchased from Xilong Chemicals (China). Ethanol and HCl were purchased from Tianjin Reagents (China). Powdered 1,2-bis(10,12-tricosadiynoyl)-*sn-glycero*-3-phosphocholine was purchased from Avanti Polar Lipids (USA). The chemicals used in this paper were of analytical grade and without further treatment. Deionized (DI) water with a resistivity of 18.2 MΩ cm (Millipore Milli-Q) was applied for solution preparation in all experiments.

2.2. Synthesis of nanotubes

2.2.1. Lipid tubule template fabrication

Powdered 1,2-bis(10,12-tricosadiynoyl)-*sn-glycero*-3-phosphocholine (1 mg) were added to 0.7 mL ethanol, followed by 0.3 mL DI water, and then manually shaken. After 5 min, the tubules were successfully fabricated, then separated by centrifugation and washed with DI water three times.

2.2.2. Fabrication of Pt nanotubes

Chloroplatinic acid (1 mL, 19 mmol/L) and 0.5 mL ascorbic acid (0.7 mol/L) were added simultaneously to 5 mL of lipid tubule solution (0.2 mg/mL) and stored at room temperature for 72 h. The suspension was centrifuged and washed with DI water. The formed NTs were then added to ethanol for 10 min to remove the template, followed by centrifugation and washing with DI water.

2.2.3. Formation of PdPt nanotubes

Chloropalladic acid (56 mmol/L) was prepared by dissolving 0.1 g palladium chloride in 9.07 mL DI water and 0.93 mL concentrated hydrochloric acid. Chloroplatinic acid (0.74 mL, 19 mmol/L), chloropalladic acid (0.26 mL, 56 mmol/L) and ascorbic acid (0.5 mL, 0.7 mol/L) were added simultaneously to 5 mL of lipid tubule solution (0.2 mg/mL) and the reaction mixture stored at room temperature for 72 h. As described earlier for the Pt NTs, the suspension was centrifuged and washed with DI water, the resultant NTs added to ethanol for 10 min to remove the template, and centrifuged again and washed with DI water.

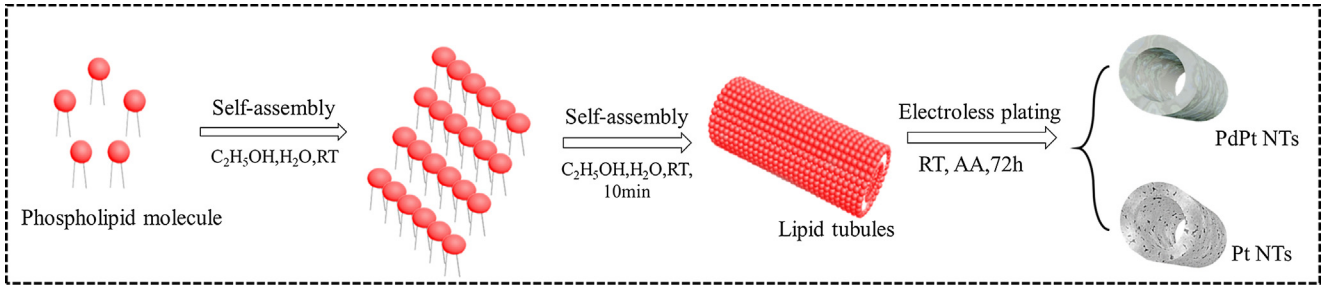

Scheme 1. Schematic illustration for the synthesis of the PtPd NTs.

2.3. Evaluation of catalytic activity

Measurement of the catalytic activity of the alloy NTs was conducted via the reduction of PNP in presence of borohydride as a reductant, performed in quartz cuvettes. The reaction procedure entailed adding PNP (3.3 mL, 0.09 mmol/L) to $NaBH_4$ (0.10 mL, 0.1 mol/L) followed by addition of 15 μg NT catalyst. Subsequently, the bright yellow solution gradually faded as the reaction proceeded and the progress was monitored periodically using a Cary 60 UV–vis spectrophotometer (Agilent, USA) focusing on the peak at 400 nm; each catalytic experiment was repeated three times.

2.4. Characterization of nanotubes

The morphology, composition, and elemental distribution of Pt and PdPt NTs was characterized by Scanning Electron Microscope (SEM) and X-ray Energy Dispersive Spectra (EDS) using a FEI Quanta 200 FEG Scanning Electron Microscopy (USA) at an accelerating voltage of 20 kV coupled with an energy-dispersive X-ray spectrometer. Fluorescence microscopy imaging was obtained with a Nikon 80i fluorescence microscope equipped with a Nikon DS-Fi1 camera (Japan). Transmission Electron Microscopy (TEM) imaging was carried out with a Hitachi H-7650 transmission electron microscope (Japan). Powder X-ray Diffraction (XRD) was measured in the reflection mode (Cu K radiation) on a D/Max-RB diffractometer. The d-spacing value was calculated using Bragg's law. X-ray Photoelectron Spectroscopy (XPS) analysis was performed using a Thermo Fisher Scientific ESCALAB 250 Xi spectrometer (USA). The deconvolution of the spectra was performed with XPS Peak 4.1 software (RCSMS lab, Hong Kong). All spectra were corrected by using the C 1s signal located at 284.5 eV. The surface compositions of alloy NTs were determined from the peak intensity and the corresponding sensitivity factors. The composition of NTs was determined by X Series 2 Inductively Coupled Plasma Optical Emission Spectrometer (ICP-OES, Thermo Scientific, USA).

3. Results and discussion

3.1. Preparation and characterization of nanotubes

The lipid tubule templates were ~12 μm in length and ~500 nm in cross-sectional diameter (Fig. S1ab); green color is derived from 1% Phospholipid dye (NBD PE) doped lipid tubule templates. Ascorbic acid was used as reducing agent due to its high water solubility, biodegradability, low toxicity compared with other reducing agents [38]. For metal plating, nanoparticle nuclei were first produced on the surface of the templates as active sites, plating was then accelerated by autocatalytic reduction [39,40]. The metal NTs were fabricated successfully after the template was removed using ethanol. It should be noted that no surfactants were used in this method. The structure and morphology of metal NTs were investigated by SEM. Fig. 1a and b show the overall morphology of metal NTs with average length of ~12 μm. As is seen from Fig. 1c, the metal NTs are tubal and their surface is smooth. EDS analysis of metal NTs (Fig. 1d) reveals only the presence of Pt in the Pt NTs. The structural features of the Pt NTs were investigated by TEM; Fig. 1e reveals a ~500 nm diameter and ~49 nm wall thickness. Fig. 1f shows that the wall is composed of network-like ultrathin nanowires of several nanometers length and ~4 nm in diameter (Fig. S2a). HR-TEM imaging reveals the lattice inter fringe distance of the Pt NTs being ~0.226 nm (Fig. 1g), corresponding to the (1 1 1) plane of face-centered-cubic (fcc) Pt crystal. Polycrystallinity is supported by the selected-area electron diffraction (SEAD) pattern (Fig. 1h).

PdPt NT SEM reveals tubal morphology with rough surface texture (Fig. 2a) and diameter of ~500 nm (Fig. 2b). Fig. 2(c and d) show that Pd and Pt components are distributed homogeneously over the NT, confirming their alloyed feature. The Pd and Pt content was determined by ICP-MS, the molar ratio of Pd to Pt was determined to be 51:49. The PdPt NT are ~57 nm in wall thickness (Fig. 2e). The wall of PdPt NT is composed of tightly but spatially cross-linked nanorod-like nanoparticles (Fig. 2f and S2a). Some irregular holes among the nanoparticles also existed, offering a large surface area, which may facilitate mass transport. HR-TEM imaging shows lattice fringe spacing distance of ~0.224 nm, indexed to (1 1 1) lattice spacing of fcc PdPt alloy crystal (Fig. 2g). This spacing is slightly smaller than observed for Pt NT, because Pd has a smaller atomic radius than Pt. The selected-area electron diffraction (SEAD) pattern further demonstrates the polycrystalline PdPt formation (Fig. 2h).

The XRD patterns in Fig. 3a reveals four diffraction peaks from the Pt and PdPt NTs, attributed to a typical fcc lattice structures. No distinct peaks for Pd or oxides are observed in the patterns, implying that a PdPt alloy was formed. Additionally, there is a

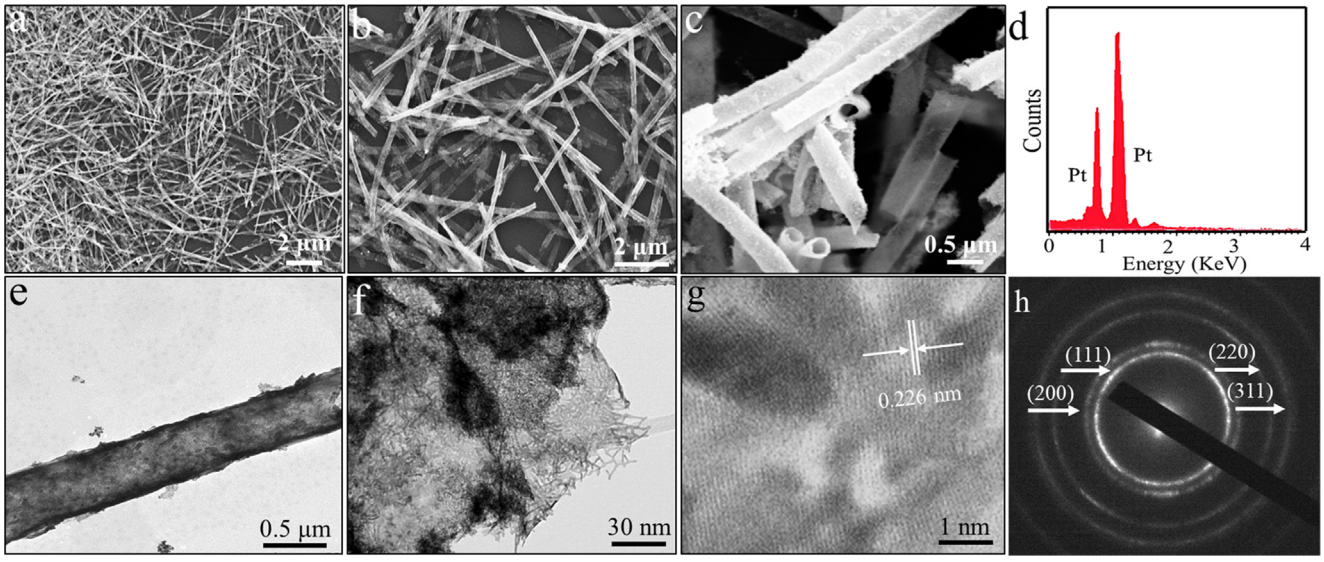

Fig. 1. (a–c) SEM images of Pt NTs, (d) the corresponding elemental mapping image, (e and f) TEM images of Pt NT, (g) high-resolution (HR) TEM image of Pt NT, (h) selected area electron diffraction (SAED) pattern of the Pt NT.

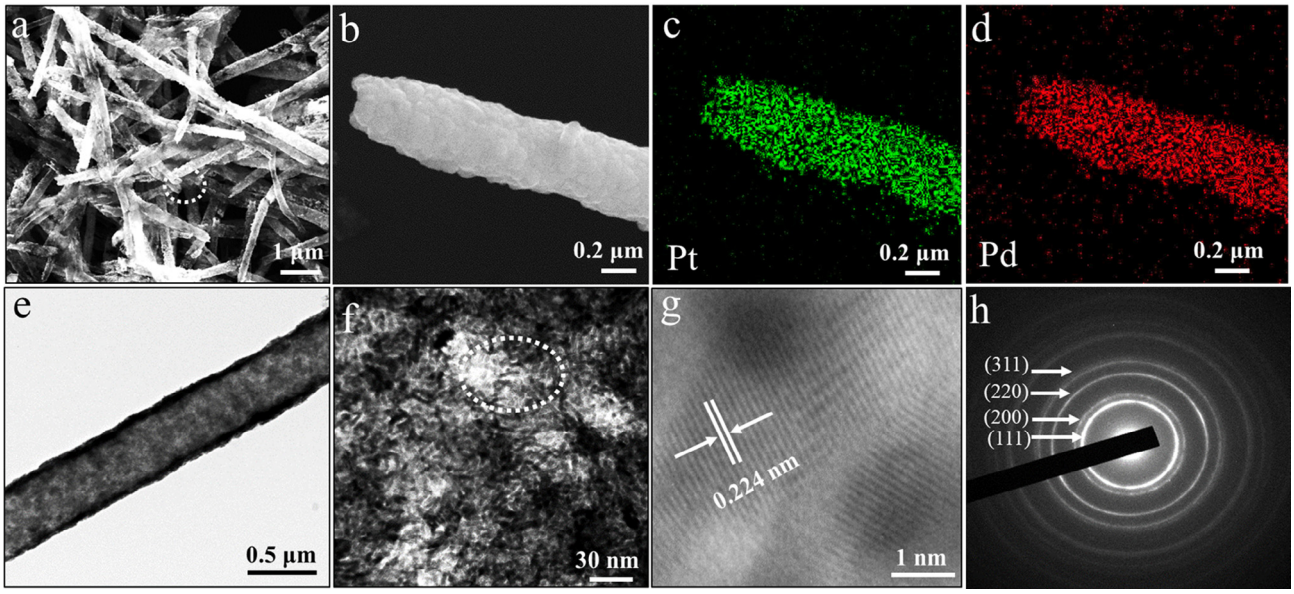

Fig. 2. (a) SEM image of PdPt NTs, (b–d) the corresponding elemental mapping images for PdPt NT, (e and f) TEM images of PdPt NT, (g) high-resolution (HR) TEM image for PdPt NT, (h) selected area electron diffraction (SAED) pattern for the PdPt NT.

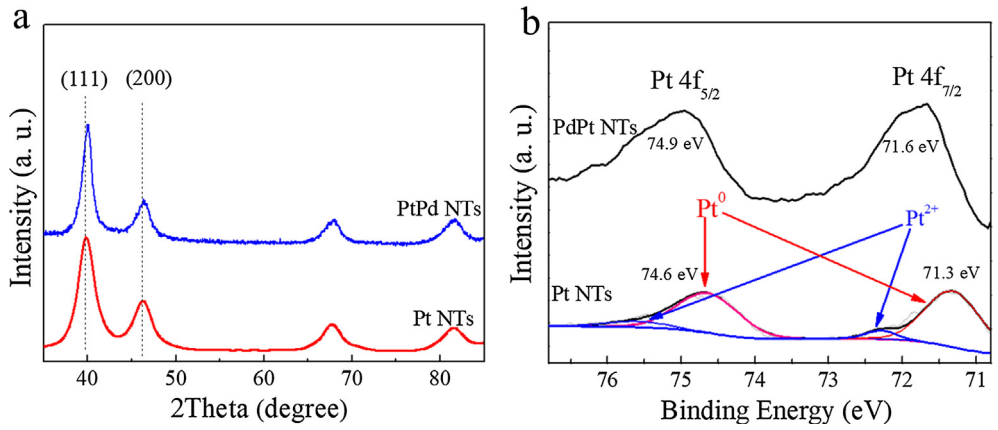

Fig. 3. (a) XRD pattern for the Pt and PdPt NTs, (b) Pt 4f XPS of the PdPt NTs.

positive shift in peak positions for the PdPt NTs compared with Pt NTs, which may be attributed to lattice strain i.e. the lattice parameters of the PdPt NTs are decreased after incorporating smaller atoms into the parent metal, giving rise to compressive strains on the crystal lattice [41].

XPS characterization was carried out to determine the elemental composition and electronic status of Pt in the NTs. For Pt NTs (Fig. 3b), two peaks at binding energies (BE) of ~71.3 and ~74.6 eV are attributed to Pt (0) $4f_{5/2}$ and $4f_{7/2}$ orbits, respectively, along with two smaller shoulder peaks at ~75.4 and 72.3 eV, assigned to Pt^{2+} species [42]. According to the intensity ratio of the Pt and Pt^{2+} peaks, that metallic Pt(0) is the predominant species in the Pt NTs. The $4f_{5/2}$ and $4f_{7/2}$ BE of Pt in the PdPt NTs was shifted to higher values. The shift of Pt $4f_{7/2}$ BE is attributed to charge transfer [43,44] (electronegativity of Pd = 2.20 and Pt = 2.28) and lattice strain [45–47].

XRD results confirm that significant compressive lattice strains exist in the PdPt NTs, which could also be responsible for the shift in BE. The difference in electronic state of Pt in the alloy may produce a positive effect on catalytic activity [48]. Fig. S2 presents the XPS results for Pd 3d. Peaks at ~341.3 and ~336.1 eV are assigned to $3d_{3/2}$ and $3d_{5/2}$ orbitals, which are ascribed to Pd^0 species [49].

3.2. Catalytic activity of the nanotubes

Hydrogenation of PNP in the presence of $NaBH_4$ is conducted to evaluate the catalytic activity of Pt and PdPt NTs at room temperature; the ensuing high pH, thereby ensuring the reduction of PNP proceeds [50]. The reduction of PNP to *p*-aminophenol (PAP) can be catalyzed by noble metals [51]; PNP aqueous solution displays a distinct UV–vis absorption peak at ~317 nm. The peak is shifted to ~400 nm after addition of $NaBH_4$, and the color of the solution becomes yellow, indicating that *p*-nitrophenolate (PAP) ions become the dominant species [50]. On addition of the Pt or PdPt NTs catalyst, the intensity of the absorption peak at ~400 nm decreased gradually as the reaction proceeds (Fig. 4). The appearance of an absorption peak at ~290 nm is attributed to PAP.[52] An isosbestic point at ~313 nm, indicates that PNP was converted to PAP without side reactions [53].

The catalytic reduction of PNP followed a first-order kinetic model [54,55].

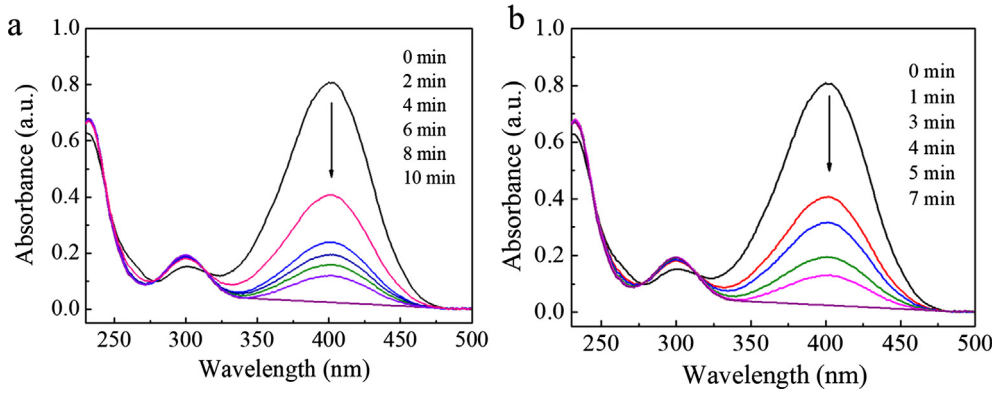

Fig. 4. The evolution of the UV–vis spectra of PNP reduction in the presence of (a) the Pt and (b) PdPt NTs.

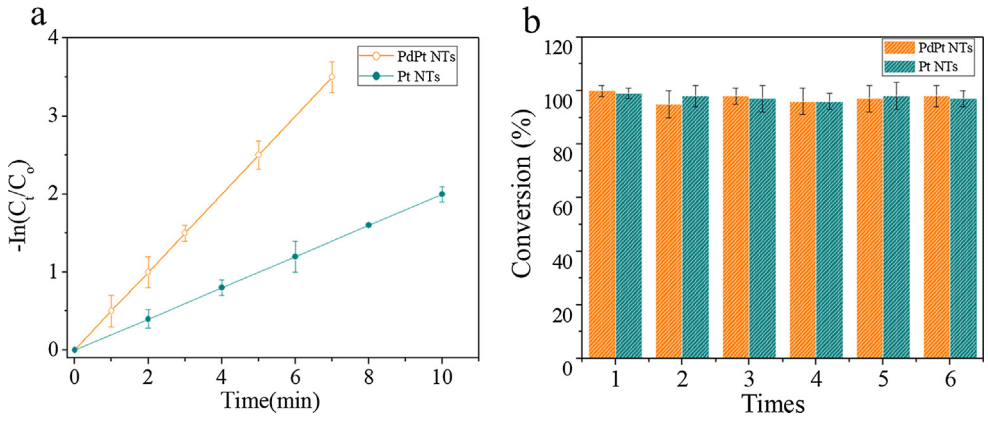

Fig. 5. (a) Plots of $\ln(C_t/C_0)$ *versus* time for PNP reduction, using the Pt and PdPt NTs as the catalysts, respectively. (b) Reusability of the Pt and PdPt NTs.

Table 1
Catalytic rate constants of the borohydride reduction of PNP using various catalysts at 20 °C.

Catalyst	PNP concentration mol L^{-1}	k_{app} min^{-1}	k_m mg^{-1} min^{-1}	Reference
Pt nanotubes	9.0×10^{-5}	0.20	13.3	This work
PdPt nanotubes	9.0×10^{-5}	0.50	33.3	This work
AuPd nanocrystal	8.7×10^{-5}	0.31	4.4	[58]
PtNi	8.5×10^{-5}	0.12	29.0	[64]
Polypyrrole/TiO_2/Pd	1.1×10^{-4}	0.74	25.0	[65]
silver nanodendrites	1.0×10^{-4}	0.34	0.2	[59]
Fe_3O_4@SiO_2–Ag	5.0×10^{-3}	0.83	0.3	[60]
Pd-Ni/rGO	5.0×10^{-3}	0.16	0.7	[61]
PtO_2/ZnO-30	1.0×10^{-2}	0.52	0.2	[62]
NiO/CuO	1.0×10^{-4}	1.50	30.1	[66]
AuNPs/r-CD	1.0×10^{-4}	0.75	0.1	[63]

$$-\frac{dc_t}{d_t} = k_{app}c_t \quad (1)$$

where c_t and k_{app} are the concentration of PNP at time t and the apparent rate constant, respectively. The concentration of PNP was proportional to its absorbance. Thus,

$$-d\ln A_t = k_{app}dt \quad (2)$$

$$-\ln(A_t/A_o) = k_{app}t \quad (3)$$

where A_t and A_0 are the absorption peak intensity of PNP at t = t min and t = 0 min, respectively.

Fig. 5a shows the correlation of $-\ln(A_t/A_0)$ *versus* time. The linear correlation indicates that the above reaction is ruled by first-order kinetics and thus k_{app} is obtained from the slope of the line. For the Pt NT tests the k_{app} was 0.2 min^{-1} and for the PdPt NT experiments it was 0.5 min^{-1} (Table 1), a 2.5-fold increase in the apparent reaction rate.

The improved catalytic activity of the PdPt NTs is attributed to the synergistic effect resulting from charge transfer and lattice strain [56] because of Pd incorporation. This causes electron transfer and structural strain, culminating in altering electron density near the Fermi level [57], thus providing new active sites. The rougher surface texture and irregular holes of the PtPd NTs may afford a larger surface area and favor mass transport, further increasing the efficiency.

Mass-normalized rate constants (k_m) can be used to compare the catalytic activity of heterogeneous catalysts; similar catalysts

reported in the literature and their data is shown in Table 1. It is revealed that the Pt NTs have greater rate mass-normalized rate constants than reported for AuPd nanocrystals [58], silver nanodendrites [59], Fe_3O_4@SiO_2–Ag [60], Pd-Ni/rGO [61], PtO_2/ZnO-30 [62] and AuNPs/r-CD [63], and the catalytic performance of PdPt NTs outperformed all those listed catalysts.

Stability is a crucial factor in evaluating the reusability of a catalyst. To assess this factor, the Pt and PtPd NTs were each utilized in six cycles for PNP reduction. The results after each cycle exhibit high catalytic performance with high conversion rates (Fig. 5b), thus indicating high stability and reusability.

4. Conclusions

A facile one-step and green protocol for Platinum (Pt) and palladium-platinum (PdPt) nanotube (NT) synthesis was reported, using lipid tubules as a template and ascorbic acid as a reducing agent. The ensuing NTs comprised of crystalline NT structures of ~12 μm length, ~500 nm cross-sectional diameter, and ~57 nm tube wall thickness. Due to an electronic effect and structural strain synergy, the PdPt NTs garnered may afford superior catalytic activity than other nanostructures previosuly reported. When applied for catalytic reduction of *p*-nitrophenol (PNP), the PdPt NTs returned an enhanced mass-normalized rate constant (k_m = 33.3 mg^{-1} min^{-1}) as compared to the Pt NTs (k_m = 13.3 mg^{-1} min^{-1}), and previously reported AuPd nanocrystals [58] (k_m = 4.4 mg^{-1} min^{-1}) and PtNi structures [64] (k_m = 29.0 mg^{-1} min^{-1}). Moreover, the NTs demonstrated high stability when used over multiple catalytic cycles. This study opens up new avenues for the fabrication of other alloy NTs (e.g. AuPt NTs, RhPt NTs) applied in catalytic processes beyond PNP reduction.

Conflict of interest

Authors declare no conflict of interest.

Acknowledgments

This work was supported by the by the National Natural Science Foundation of China (21473045), National Water Pollution Control and Treatment Science and Technology Major Project (Grant No. 2018ZX07109-003).

Appendix A. Supplementary material

Supplementary data to this article can be found online at https://doi.org/10.1016/j.jcis.2018.12.053.

References

[1] Z. Shen, J. Zhang, D. Hou, D.C.W. Tsang, Y.S. Ok, D.S. Alessi, Synthesis of MgO-coated corncob biochar and its application in lead stabilization in a soil washing residue, Environ. Int. (2018).
[2] Z. Shen, D. Hou, W. Xu, J. Zhang, F. Jin, B. Zhao, S. Pan, T. Peng, D.S. Alessi, Assessing long-term stability of cadmium and lead in a soil washing residue amended with MgO-based binders using quantitative accelerated ageing, Sci. Total Environ. 643 (2018) 1571–1578.
[3] Z. Shen, D. Hou, F. Jin, J. Shi, X. Fan, D.C.W. Tsang, D.S. Alessi, Effect of production temperature on lead removal mechanisms by rice straw biochars, Sci. Total Environ. 655 (2019) 751–758.
[4] D. O'Connor, D. Hou, Y.S. Ok, Y. Song, A.K. Sarmah, X. Li, F.M.G. Tack, Sustainable in situ remediation of recalcitrant organic pollutants in groundwater with controlled release materials: A review, J. Controlled Release 283 (2018) 200–213.
[5] T. Peng, D. O'Connor, B. Zhao, Y. Jin, Y. Zhang, L. Tian, N. Zheng, X. Li, D. Hou, Spatial distribution of lead contamination in soil and equipment dust at children's playgrounds in Beijing, China, Environ. Pollut. 245 (2019) 363–370.
[6] Z. Shen, D. Hou, P. Zhang, Y. Wang, Y. Zhang, P. Shi, D. O'Connor, Lead-based paint in children's toys sold on China's major online shopping platforms, Environ. Pollut. 241 (2018) 311–318.
[7] M. Campelo Juan, D. Luna, R. Luque, M. Marinas José, A. Romero Antonio, Sustainable preparation of supported metal nanoparticles and their applications in catalysis, ChemSusChem 2 (1) (2009) 18–45.
[8] C. Mihut, C. Descorme, D. Duprez, M.D. Amiridis, Kinetic and spectroscopic characterization of cluster-derived supported Pt–Au catalysts, J. Catal. 212 (2) (2002) 125–135.
[9] J. Zhang, G. Chen, D. Guay, M. Chaker, D. Ma, Highly active PtAu alloy nanoparticle catalysts for the reduction of 4-nitrophenol, Nanoscale 6 (4) (2014) 2125–2130.
[10] Y. Liu, B. Liu, Y. Liu, Q. Wang, W. Hu, P. Jing, L. Liu, S. Yu, J. Zhang, Improvement of catalytic performance of preferential oxidation of CO in H_2-rich gases on three-dimensionally ordered macro- and meso-porous Pt–Au/CeO_2 catalysts, Appl. Catal. B: Environ. 142–143 (2013) 615–625.
[11] C. Xu, Y. Du, C. Li, J. Yang, G. Yang, Insight into effect of acid/base nature of supports on selectivity of glycerol oxidation over supported Au-Pt bimetallic catalysts, Appl. Catal. B: Environ. 164 (2015) 334–343.
[12] N. Pradhan, A. Pal, T. Pal, Catalytic reduction of aromatic nitro compounds by coinage metal nanoparticles, Langmuir 17 (5) (2001) 1800–1802.
[13] Y.Y. Chu, Y. Qian, W.J. Wang, X.L. Deng, A dual-cathode electro-Fenton oxidation coupled with anodic oxidation system used for 4-nitrophenol degradation, J. Hazard. Mater. 199–200 (2012) 179–185.
[14] A.A. Al-Kahtani, T. Almuqati, N. Alhokbany, T. Ahamad, M. Naushad, S.M. Alshehri, A clean approach for the reduction of hazardous 4-nitrophenol using gold nanoparticles decorated multiwalled carbon nanotubes, J. Clean. Prod. 191 (2018) 429–435.
[15] S. Haydar, M.A. Ferro-Garcıa, J. Rivera-Utrilla, J.P. Joly, Adsorption of p-nitrophenol on an activated carbon with different oxidations, Carbon 41 (3) (2003) 387–395.
[16] L.L. Bo, Y.B. Zhang, X. Quan, B. Zhao, Microwave assisted catalytic oxidation of p-nitrophenol in aqueous solution using carbon-supported copper catalyst, J. Hazard. Mater. 153 (3) (2008) 1201–1206.
[17] A. O'Connor Owen, L.Y. Young, Toxicity and anaerobic biodegradability of substituted phenols under methanogenic conditions, Environ. Toxicol. Chem. 8 (10) (1989) 853–862.
[18] M. Thakur, G. Sharma, T. Ahamad, A.A. Ghfar, D. Pathania, M. Naushad, Efficient photocatalytic degradation of toxic dyes from aqueous environment using gelatin-Zr(IV) phosphate nanocomposite and its antimicrobial activity, Colloids Surf. B: Biointerfaces 157 (2017) 456–463.
[19] H. Zhang, C. Fei, D. Zhang, F. Tang, Degradation of 4-nitrophenol in aqueous medium by electro-Fenton method, J. Hazard. Mater. 145 (1) (2007) 227–232.
[20] N. Modirshahla, M.A. Behnajady, S. Mohammadi-Aghdam, Investigation of the effect of different electrodes and their connections on the removal efficiency of 4-nitrophenol from aqueous solution by electrocoagulation, J. Hazard. Mater. 154 (1) (2008) 778–786.
[21] P. Cañizares, C. Sáez, J. Lobato, M.A. Rodrigo, Electrochemical treatment of 4-nitrophenol-containing aqueous wastes using boron-doped diamond anodes, Indus. Eng. Chem. Res. 43 (9) (2004) 1944–1951.
[22] B. Lai, Y. Zhang, Z. Chen, P. Yang, Y. Zhou, J. Wang, Removal of p-nitrophenol (PNP) in aqueous solution by the micron-scale iron–copper (Fe/Cu) bimetallic particles, Appl. Catal. B: Environ. 144 (2014) 816–830.
[23] P. Zhang, D. Hou, D. O'Connor, X. Li, S. Pehkonen, R.S. Varma, X. Wang, Green and size-specific synthesis of stable Fe–Cu oxides as earth-abundant adsorbents for malachite green removal, ACS Sustain. Chem. Eng. 6 (7) (2018) 9229–9236.
[24] H. Zhu, S. Zhang, S. Guo, D. Su, S. Sun, Synthetic control of FePtM nanorods (M = Cu, Ni) to enhance the oxygen reduction reaction, J. Am. Chem. Soc. 135 (19) (2013) 7130.
[25] S. Guo, S. Sun, FePt nanoparticles assembled on graphene as enhanced catalyst for oxygen reduction reaction, J. Am. Chem. Soc. 134 (5) (2012) 2492–2495.
[26] X. Jin, B. He, J. Miao, J. yuan, Q. Zhang, L. Niu, Stabilization and dispersion of PtRu and Pt nanoparticles on multiwalled carbon nanotubes using phosphomolybdic acid, and the use of the resulting materials in a direct methanol fuel cell, Carbon 50 (8) (2012) 3083–3091.
[27] D. O'Connor, D. Hou, Targeting cleanups towards a more sustainable future, Environ. Sci.: Process. Impacts (2018).
[28] D. O'Connor, T. Peng, G. Li, S. Wang, L. Duan, J. Mulder, G. Cornelissen, Z. Cheng, S. Yang, D. Hou, Sulfur-modified rice husk biochar: A green method for the remediation of mercury contaminated soil, Sci. Total Environ. 621 (2018) 819–826.
[29] D. Hou, Y. Song, J. Zhang, M. Hou, D. O'Connor, M. Harclerode, Climate change mitigation potential of contaminated land redevelopment: A city-level assessment method, J. Clean Prod. 171 (2018) 1396–1406.
[30] A. Kalaiselvi, S.M. Roopan, G. Madhumitha, C. Ramalingam, G. Elango, Synthesis and characterization of palladium nanoparticles using Catharanthus roseus leaf extract and its application in the photo-catalytic degradation, Spectrochim. Acta A Mol. Biomol. Spectrosc. 135 (2015) 116–119.
[31] H. Yang, X. Liu, S. Sun, Y. Nie, H. Wu, T. Yang, S. Zheng, S. Lin, Green and facile synthesis of graphene nanosheets/$K_3PW_{12}O_{40}$ nanocomposites with enhanced photocatalytic activities, Mater. Res. Bull. 78 (2016) 112–118.
[32] T. Kijima, T. Yoshimura, M. Uota, T. Ikeda, D. Fujikawa, S. Mouri, S. Uoyama, Noble-metal nanotubes (Pt, Pd, Ag) from lyotropic mixed-surfactant liquid-crystal templates, Angewandte Chemie Int. Ed. 116 (2) (2010) 230–234.
[33] C. Zhu, D. Du, A. Eychmüller, Y. Lin, Engineering ordered and nonordered porous noble metal nanostructures: Synthesis, assembly, and their applications in electrochemistry, Chem. Rev. 115 (16) (2015) 8896–8943.

[34] Y. Zhou, Lipid nanotubes as scaffold toward construction of one-dimensional nanostructures, Sci. Adv. Mater. 2 (3) (2010) 359–364.
[35] M.R. Jones, K.D. Osberg, R.J. Macfarlane, M.R. Langille, C.A. Mirkin, Templated techniques for the synthesis and assembly of plasmonic nanostructures, Chem. Rev. 111 (6) (2011) 3736–3827.
[36] X. Yang, H. Tang, K. Cao, H. Song, W. Sheng, Q. Wu, Templated-assisted one-dimensional silica nanotubes: synthesis and applications, J. Mater. Chem. 21 (17) (2011) 6122–6135.
[37] M. Assali, J.-J. Cid, I. Fernández, N. Khiar, Supramolecular diversity through click chemistry: Switching from nanomicelles to 1D-nanotubes and tridimensional hydrogels, Chem. Mater. 25 (21) (2013) 4250–4261.
[38] M.N. Nadagouda, R.S. Varma, A greener synthesis of core (Fe, Cu)-shell (Au, Pt, Pd, and Ag) nanocrystals using aqueous vitamin C, Cryst. Growth Des. 7 (12) (2007) 2582–2587.
[39] S. Sun, F. Jaouen, J.-P. Dodelet, Controlled growth of Pt nanowires on carbon nanospheres and their enhanced performance as electrocatalysts in PEM fuel cells, Adv. Mater. 20 (20) (2008) 3900–3904.
[40] Y.N. Wang, S.H. Ma, Q.C. Li, Y. Zhang, X.J. Wang, X.J. Han, Hollow platinum nanospheres and nanotubes templated by shear flow-induced lipid vesicles and tubules and their applications on hydrogen evolution, ACS Sustain. Chem. Eng. 4 (7) (2016) 3773–3779.
[41] Y. Shen, Z. Zhang Mr, K. Xiao, J. Xi, Synthesis of Pt, PtRh, and PtRhNi alloys supported by pristine graphene nanosheets for ethanol electrooxidation, ChemCatChem 6 (11) (2014) 3254–3261.
[42] Y. Jiang, A.J. O'Neill, Y. Ding, Zinc oxide nanoparticle-coated films: fabrication, characterization, and antibacterial properties, J. Nanoparticle Res. 17 (4) (2015) 180.
[43] M.A. Rigsby, W.-P. Zhou, A. Lewera, H.T. Duong, P.S. Bagus, W. Jaegermann, R. Hunger, A. Wieckowski, Experiment and theory of fuel cell catalysis: Methanol and formic acid decomposition on nanoparticle Pt/Ru, J. Phys. Chem. C 112 (39) (2008) 15595–15601.
[44] Y. Shen, M.Z. Zhang, K. Xiao, J. Xi, Synthesis of Pt, PtRh, and PtRhNi alloys supported by pristine graphene nanosheets for ethanol electrooxidation, ChemCatChem 6 (11) (2014) 3254–3261.
[45] X. Ge, X. Yan, R. Wang, F. Tian, Y. Ding, Tailoring the structure and property of pt-decorated nanoporous gold by thermal annealing, J. Phys. Chem. C 113 (17) (2009) 7379–7384.
[46] P.S. Bagus, C.J. Nelin, E.S. Ilton, M. Baron, H. Abbott, E. Primorac, H. Kuhlenbeck, S. Shaikhutdinov, H.J. Freund, The complex core level spectra of CeO_2: An analysis in terms of atomic and charge transfer effects, Chem. Phys. Lett. 487 (4–6) (2010) 237–240.
[47] J. Liu, L. Cao, W. Huang, Z. Li, Preparation of AuPt alloy foam films and their superior electrocatalytic activity for the oxidation of formic acid, ACS Appl. Mater. Interf. 3 (9) (2011) 3552–3558.
[48] W.P. Zhou, A. Lewera, R. Larsen, R.I. Masel, P.S. Bagus, A. Wieckowski, Size effects in electronic and catalytic properties of unsupported palladium nanoparticles in electrooxidation of formic acid, J. Phys. Chem. B 110 (27) (2006) 13393–13398.
[49] D.B. Huang, Q. Yuan, H.H. Wang, Z.Y. Zhou, Facile synthesis of PdPt nanoalloys with sub-2.0 nm islands as robust electrocatalysts for methanol oxidation, Chem. Commun. (Camb) 50 (88) (2014) 13551–13554.
[50] K. Esumi, R. Isono, T. Yoshimura, Preparation of PAMAM– and PPI–metal (silver, platinum, and palladium) nanocomposites and their catalytic activities for reduction of 4-nitrophenol, Langmuir 20 (1) (2004) 237–243.
[51] S. Saha, A. Pal, S. Kundu, S. Basu, T. Pal, Photochemical green synthesis of calcium-alginate-stabilized ag and au nanoparticles and their catalytic application to 4-nitrophenol reduction, Langmuir 26 (4) (2010) 2885–2893.
[52] N. Pradhan, A. Pal, T. Pal, Silver nanoparticle catalyzed reduction of aromatic nitro compounds, Colloids Surf. A: Physicochem. Eng. Asp. 196 (2) (2002) 247–257.
[53] L. Joongoo, P.J. Chan, S. Hyunjoon, A nanoreactor framework of a Au@SiO_2 yolk/shell structure for catalytic reduction of p-nitrophenol, Adv. Mater. 20 (8) (2008) 1523–1528.
[54] Y. Lu, Y. Mei, M. Drechsler, M. Ballauff, Thermosensitive core–shell particles as carriers for Ag nanoparticles: modulating the catalytic activity by a phase transition in networks, Angewandte Chemie Int. Ed. 45 (5) (2006) 813–816.
[55] Y. Mei, Y. Lu, F. Polzer, M. Ballauff, M. Drechsler, Catalytic activity of palladium nanoparticles encapsulated in spherical polyelectrolyte brushes and core−shell microgels, Chem. Mater. 19 (5) (2007) 1062–1069.
[56] Y.J. Tong, Unconventional promoters of catalytic activity in electrocatalysis, Chem. Soc. Rev. 41 (24) (2012) 8195–8209.
[57] S. Sun, G. Zhang, D. Geng, Y. Chen, R. Li, M. Cai, X. Sun, A highly durable platinum nanocatalyst for proton exchange membrane fuel cells: Multiarmed starlike nanowire single crystal, Angewandte Chemie Int. Ed. 50 (2) (2010) 422–426.
[58] J. Zhang, C. Hou, H. Huang, L. Zhang, Z. Jiang, G. Chen, Y. Jia, Q. Kuang, Z. Xie, L. Zheng, Surfactant-concentration-dependent shape evolution of Au–Pd alloy nanocrystals from rhombic dodecahedron to trisoctahedron and hexoctahedron, Small 9 (4) (2012) 538–544.
[59] W. Zhang, F. Tan, W. Wang, X. Qiu, X. Qiao, J. Chen, Facile, template-free synthesis of silver nanodendrites with high catalytic activity for the reduction of p-nitrophenol, J. Hazard. Mater. 217–218 (2012) 36–42.
[60] X. Du, J. He, J. Zhu, L. Sun, S. An, Ag-deposited silica-coated Fe_3O_4 magnetic nanoparticles catalyzed reduction of p-nitrophenol, Appl. Surf. Sci. 258 (7) (2012) 2717–2723.
[61] T.A. Revathy, S. Dhanavel, T. Sivaranjani, V. Narayanan, T. Maiyalagan, A. Stephen, Highly active graphene-supported palladium-nickel alloy nanoparticles for catalytic reduction of 4-nitrophenol, Appl. Surf. Sci. 449 (2018) 764–771.
[62] X. Yang, Y. Li, P. Zhang, R. Zhou, H. Peng, D. Liu, J. Gui, Photoinduced in situ deposition of uniform and well-dispersed PtO_2 nanoparticles on ZnO nanorods for efficient catalytic reduction of 4-nitrophenol, ACS Appl. Mater. Interf. 10 (27) (2018) 23154–23162.
[63] B. Zheng, X. Liu, Y. Wu, L. Yan, J. Du, J. Dai, Q. Xiong, Y. Guo, D. Xiao, Surfactant-free gold nanoparticles: rapid and green synthesis and their greatly improved catalytic activities for 4-nitrophenol reduction, Inorg. Chem. Front. 4 (8) (2017) 1268–1272.
[64] S.K. Ghosh, M. Mandal, S. Kundu, S. Nath, T. Pal, Bimetallic Pt–Ni nanoparticles can catalyze reduction of aromatic nitro compounds by sodium borohydride in aqueous solution, Appl. Catal. A: Gener. 268 (1) (2004) 61–66.
[65] X. Lu, X. Bian, G. Nie, C. Zhang, C. Wang, Y. Wei, Encapsulating conducting polypyrrole into electrospun TiO2 nanofibers: a new kind of nanoreactor for in situ loading Pd nanocatalysts towards p-nitrophenol hydrogenation, J. Mater. Chem. 22 (25) (2012) 12723–12730.
[66] G. Wu, X. Liang, L. Zhang, Z. Tang, M. Al-Mamun, H. Zhao, X. Su, Fabrication of highly stable metal oxide hollow nanospheres and their catalytic activity toward 4-nitrophenol reduction, ACS Appl. Mater. Interf. 9 (21) (2017) 18207–18214.